

A NEW DIAGNOSTIC METHOD FOR ASSESSMENT OF STELLAR STRATIFICATION IN STAR CLUSTERS

DIMITRIOS A. GOULIERMIS

Max-Planck-Institut für Astronomie, Königstuhl 17, D-69117 Heidelberg, Germany
dgoulie@mpia.de

AND

RICHARD DE GRIJS AND YU XIN

Department of Physics & Astronomy, The University of Sheffield, Hicks Building, Hounsfield Road, Sheffield S3 7RH, UK
R.deGrijs@sheffield.ac.uk; xinyu@bao.ac.cn

Accepted for Publication in the Astrophysical Journal, 6 November 2008

ABSTRACT

We propose a new method for the characterization of stellar stratification in stellar systems. The method uses the mean-square radius (also called the *Spitzer radius*) of the system as a diagnostic tool. An estimate of the observable counterpart of this radius for stars of different magnitude ranges is used as the *effective radius* of each stellar species in a star cluster. We explore the dependence of these radii on magnitude as a possible indication of stellar stratification. This method is the first of its kind to use a dynamically stable radius, and though seemingly trivial it has never been applied before. We test the proposed method using model star clusters, which are constructed to be segregated on the basis of a Monte Carlo technique, and on *Hubble Space Telescope* observations of mass-segregated star clusters in order to explore the limitations of the method in relation to actual data. We conclude that the method performs efficiently in the detection of stellar stratification and its results do not depend on the data, provided that incompleteness has been accurately measured and the contamination by the field population has been thoroughly removed. Our diagnosis method is also independent of any model or theoretical prediction, in contrast to the ‘classical’ methods used so far for the detection of mass segregation.

Subject headings: Galaxies: star clusters – Magellanic Clouds – stellar dynamics – Methods: statistical

1. INTRODUCTION

Mass segregation or *stellar stratification* is the phenomenon, according to which the massive stars in a star cluster are mostly concentrated toward its center. Due to dynamical evolution massive stars move inwards to the center of the cluster through two-body interactions. Due to the same process less massive stars may move outwards, so that on average the system ‘evaporates’ (e.g., Lightman & Shapiro 1978; Meylan & Heggie 1997). This is more commonly known as *dynamical mass segregation*. However, mass segregation is also being observed in dynamically young stellar systems, supposedly due to the formation of massive stars closer to the center of the newly-born system (e.g., Murray & Lin 1996; Bonnell & Davies 1998). This type of mass segregation is usually referred to as *primordial*.

Both types of stellar stratification affect the physical properties of the cluster in a manner which allows us to develop diagnostic tools for its detection and quantification. Such tools involve the identification of changes in the surface density profiles and the mass functions of the clusters, or of the core radii of stars in different mass groups. Specifically, stellar stratification in a star cluster can be detected from the surface density profiles of stars in different brightness ranges. If f is the stellar surface density (for every brightness range) within a distance R from the center of the cluster, then $f(R)$ can be used as an indication of stratification at the magnitude limit, where it changes significantly (e.g., Scaria & Bappu 1981; Sagar et al. 1988; Subramaniam et al. 1993; Kontizas et al. 1998). The density profiles can be approximated by $\log f \propto \gamma \log R$ (Elson et al. 1987) and the slope, γ , can be used to quantify any significant change in $f(R)$. Although this approximation was well designed, in practice peculiarities of the density profiles toward the center of clusters that are not completely spheri-

cal tend to produce large uncertainties in γ , which hide any potential mass segregation (see, e.g., Gouliermis et al. 2004).

Another well-applied method is the construction of the luminosity or mass function (LF, MF) of the cluster and the investigation of its radial dependence (e.g., Pandey et al. 1992; King et al. 1995; Fischer et al. 1998; Kontizas et al. 1998, de Grijs et al. 2002a,b). If the cluster is indeed segregated, then the appearance of more massive stars toward its center will result in shallower LFs and MFs toward smaller radii (e.g., de Grijs et al. 2002a). However, this method has several constraints imposed by the difficulties in the construction of an accurate MF based on the use of theoretical mass-luminosity (ML) relations. The use of different ML relations may result in significant differences in the MF slopes obtained, independently of whether any mass segregation is actually present (de Grijs et al. 2002b). In addition, the investigation of any radial dependence of the LF and MF slopes is not as straightforward as it seems, since its detection is rather sensitive to the radial distance range being considered, i.e., where the slope is to be estimated (Gouliermis et al. 2004).

A rather interesting method is based on the use of the core radius of the cluster as estimated for stars in specific magnitude (or mass) ranges (e.g., Brandl et al. 1996; de Grijs et al. 2002b). Core radii can be derived from the corresponding stellar number-density profiles by fitting to the latter the models of Elson et al. (1987) and by approximating them to the canonical King models for Galactic globular clusters (King 1966). However, this method seems to be model-dependent to a degree, which makes its application difficult. Another proposed method is to measure the mean stellar mass within a given radius (e.g., Bonnell & Davies 1998; Hillenbrand & Hartmann 1998), but this diagnostic requires accurate knowledge of the stellar masses, which is not always feasible (de

Grijs et al. 2002b; Gouliermis et al. 2004).

For the methods discussed above, detecting stellar stratification requires observations at high resolution, so that detailed radial density distributions for the fainter magnitude ranges and complete MFs in several annuli around the center of the cluster can be constructed accurately. These methods can provide useful information about the segregated masses as well as on the radius up to which the cluster is shown to be segregated. However, it seems that all of these methods are very sensitive to the quality of the observed data, as well as to model assumptions. Moreover, all of the methods for the detection of stellar stratification used thus far are closely associated to the fitting of predefined functions to the data and searching for parametric differences in these functions. One such method, for example, involves the study of the stellar projected density distribution of stars of different magnitudes; here, the differences in the exponents of the slopes fitted are seen as proof of mass segregation. A second method is based on the inherently imperfect derivation of radius-dependent MFs, while yet another makes use of the core radius of the system for different stellar groups, relying on apparent structures, but it is extensively model-dependent. The problem that all these studies suffer from is that *it is very difficult to compare their results among each other, thus leading to extensive discussions about the nature and even the reality of stellar stratification.*

In this paper we present a robust method for the detection of stellar stratification. The simple application of this method can yield direct information about the spatial extent (radial distribution) of stellar groups in different magnitude (mass) ranges. It is based on the notion of a dynamically stable radius of a star cluster, the so-called ‘*Spitzer radius*,’ and leads to an observed ‘*effective radius*.’ The diagnostic method for stellar stratification is described in § 2. The diagnostic process is applied to and tested on a set of simulated spherical star clusters in § 3, which are constructed on the basis of Monte Carlo simulations. We thus validate the use of the diagnostic and the unavoidable constraints. We then apply the method to real data of two intermediate-age clusters in the Magellanic Clouds observed with the *Advanced Camera for Surveys* (ACS) on-board the *Hubble Space Telescope* (HST), and we report on our results in § 4. A comparison of the results of our method with those of the classical method of the MF dependence for the test clusters is also presented in § 4. Conclusions and a discussion on the use of this diagnostic tool are summarized in § 5.

2. DIAGNOSTIC FOR SPATIAL STELLAR STRATIFICATION

2.1. The Spitzer Radius

The radius commonly known as the ‘*Spitzer Radius*’ of a star cluster was introduced by L. Spitzer Jr. and his collaborators, who used it as a distance indicator for different stellar subclasses in a cluster (see, e.g., Spitzer 1958). Since gravity operates proportional to the inverse square of the distance between a dynamical center and a subject mass, if the latter represents a group of masses distributed around the center (e.g., stars in a cluster), then the square distance of this group can be replaced by the mean-square distance of its members. Specifically, the gravitational force in a spherical stellar system at a distance r from its center, is (e.g., Spitzer 1958, 1969)

$$\frac{dV}{dr} = \frac{GM_r}{r^2}, \quad (1)$$

where V is the potential and M_r the mass contained within a radius r . King (1965) showed that considering only one single type of stars with mass m and if $S(x)dx$ is the number of stars in a strip of width dx , then assuming a Plummer (1911) stellar distribution, the potential is

$$V(r) = -\frac{2Gm}{r} \int_0^r S(x)dx. \quad (2)$$

Furthermore, Spitzer, investigating energy equipartition between two different mass groups, notes that the term r^2 in Eq. (1) may be expressed as the mean value of the square distance of all stars in a single mass group, if they were the only cluster members. Consequently, the square root of this value gives r in Eq. (2). This radius, later called the ‘*Spitzer radius*,’ corresponds to the distance up to which the stars of this specific mass group affect the gravitational field of the cluster as a whole.

Therefore, the Spitzer radius of a star cluster is defined as the mean-square distance of the stars from its center,

$$r_{\text{Sp}} = \sqrt{\frac{\sum_{i=1}^N r_i^2}{N}}, \quad (3)$$

where r_i is the radial distance of the i^{th} star and N is the total number of stars. For a Maxwellian distribution of a group of masses in a parabolic potential well, which represents that of a globular cluster very well, the half-mass radius of the system is almost equal to ($\sim 90\%$ of) the Spitzer radius (Spitzer 1969). Consequently, considering the limitations in the measurement of the half-mass radius of a cluster versus the direct measurement of the Spitzer radius, the latter can be considered quite important in relation to the dynamical status of the cluster, being used as its characteristic radius.

As far as stellar stratification is concerned, in a star cluster displaying mass segregation one should be able to observe the more massive stars concentrated toward the center of the system by plotting the position coordinates of the stars according to their magnitudes. The Spitzer radius, being a dynamically stable radius, can be used for the parameterization of the spatial distribution of stars in different brightness ranges. Based on this assumption, we propose here a method according to which stellar stratification in a star cluster can be quantified directly by estimating the corresponding Spitzer radius for every group of magnitudes, using Eq. (3). This simple approach provides information on both *where* in the cluster every stellar-luminosity group is confined, and at *which brightness* stellar stratification occurs.

2.2. Spitzer Radius and Stellar Stratification

We test the hypothesis outlined above on artificial populous spherical clusters that we constructed based on the use of the Monte Carlo technique. The proposed method is mainly designed for the identification of stellar stratification in clusters in the Magellanic Clouds (MCs), and therefore the simulated clusters are taken to have structural parameters similar to those in the MCs. Results based on observations of MCs clusters with *HST* are particularly considered due to their deepness and spatial resolution. Specifically, a sample of four star clusters (NGC 1818, NGC 2004, NGC 2100, and NGC 330) observed by Keller et al. (2000) with the *Wide-Field Planetary Camera 2* (WFPC2) is used as an initial guideline in our simulations, by considering their structural parameters for the

artificial star clusters we construct here. As a consequence, our simulated clusters have tidal radii of $r_t \simeq 2'0$, while King models with $C = \log r_t/r_c \sim 1.0$ are assumed to represent their density profiles. The corresponding core radii, r_c , of the artificial clusters have values within the limits given by Mackey & Gilmore (2003a,b), who compiled two-color *HST* observations for a sample of 53 and 10 rich star clusters in the Large and Small Magellanic Cloud (LMC, SMC), respectively.

The LFs of the simulated clusters are selected as variations of a global LF, which was constructed based on the observed LFs of the clusters in the sample of Gouliermis et al. (2004). This global LF is found to be in very good agreement with the LFs of star clusters in the MCs as determined using *HST* imaging by other authors (e.g., de Grijs et al. 2002c: NGC 1805, NGC 1818, NGC 1831, NGC 1868, NGC 2209, and Hodge 14; Sirianni et al. 2002: NGC 330; Testa et al. 1999, Brocato et al. 2003: NGC 1866; Santiago et al. 2001: NGC 1805, NGC 1818, NGC 1831, NGC 1868, and NGC 2209). An example of three artificial clusters with different LFs is given in Fig. 1. The LF in each case is also given at the bottom panel of the figure. All three clusters have the same tidal radius and the same degree of stratification, but the differences in their LFs are fed through to their stellar numbers and consequently to their appearance.

Stellar stratification was considered for our artificial star clusters. Hence, several degrees of segregation (including no segregation) were adopted. This was done using a projected limiting radius within which each stellar group should be confined. Based on our hypothesis, stellar stratification in these clusters should be detected through the dependence of the estimated Spitzer radius of stars in specific magnitude ranges versus the corresponding mean magnitude. Indeed, our tests show that the initially assumed stellar stratification (of any degree) is reconstructed by the plot of Spitzer radii per magnitude range versus magnitude for all artificial star clusters considered. In Fig. 2 we show a sample of three degrees of stratification for the same simulated cluster (similar to the middle panel in Fig. 1). Spitzer radii in this figure are normalized for reasons of comparability. Three different symbols were used for the plot, as if the cluster was observed projected onto the xy , xz , or yz plane, respectively.

2.3. Spitzer Radius of Observed Star Clusters

Identical to the concept discussed in the previous sections, observations of the radial distribution of stars in a real star cluster give us a relation of the kind of Eq. (3),

$$r_{\text{obs}} = \sqrt{\frac{\sum_{i=1}^{N_{\text{obs}}} r_i^2}{N_{\text{obs}}}}. \quad (4)$$

However, this distribution is significantly affected by two important observational constraints: (i) incompleteness of the stellar sample and (ii) contamination by field stars. To obtain an accurate measurement of the observed Spitzer radii per magnitude range in a cluster, both these constraints should be considered.

2.3.1. Incompleteness of the observations

The observed stellar samples in star clusters are incomplete due to the observations. Although this can lead to a parameterization significantly differing from reality, the bias

introduced to the data analysis is, in general, well understood. Consequently, solving the problem of incompleteness is a more or less straightforward procedure, which takes place through extensive artificial-star tests (e.g. de Grijs et al. 2002a; Gouliermis et al. 2004). A set of artificial stars is generated within each of the observed frames. Then, an identical reduction procedure is performed on the artificially enriched frames, in order to estimate the number of the ‘recovered’ artificial stars. The completeness factor C is the ratio between the number of stars recovered to the number of stars originally simulated. This factor depends on the brightness of the stars and their positions in the cluster. Therefore, an effective completeness estimation for a stellar cluster requires that incompleteness is calculated for stars in different magnitude bins and for different distances from the center of the cluster.

In order to correct the observed Spitzer radius for incompleteness, for every counted star its completeness factor is calculated according to its magnitude and radial distance. If the radial distance of the i^{th} star is r_i and its corresponding completeness factor is C_i then we assign $1/C_i$ stars to this distance and the total number of counted stars is affected accordingly. Thus, the completeness-corrected observed Spitzer radius should be

$$r_{\text{obs,cc}} = \sqrt{\frac{\sum_{i=1}^{N_{\text{obs}}} (r_i^2/C_i)}{\sum_{i=1}^{N_{\text{obs}}} (1/C_i)}}. \quad (5)$$

2.3.2. Contribution from the field populations.

The contamination of the observations by the field populations is probably the most difficult problem to be dealt with. Theoretically, if even one massive field star was counted as a cluster member and if it is far away from the center of the cluster, then the measured radius would be overestimated. In the same context, with comprehensive observations of the field we know the expected number of contaminating stars per magnitude range, but we still cannot know their position, which is the most important constraint as far as the radius estimation is concerned.

One may confront this problem by first defining the largest radial distance among the stars of the entire sample in a specific magnitude bin and then normalizing the known surface density of field stars in this magnitude range to the surface confined by this radius. Hence, one could obtain a good estimation of the number of field stars expected to contaminate this area in the specific magnitude range, and correct for field contribution by subtracting the appropriate fraction of the total number of field stars. If, for example, there are N_F field stars expected in a total number, N , of stars in a specific magnitude range (within a maximum radial distance, r_{max}), then we can subtract their fraction $F = N_F/N < 1$ from every counted star with distance $r_i \leq r_{\text{max}}$. Then, the field-subtracted observed Spitzer radius, ignoring for the moment any incompleteness corrections, derived from Eq. (4) for stars in every magnitude range should be

$$r_{\text{obs,fs}} = \sqrt{\frac{\sum_{i=1}^{N_{\text{obs}}} [(1-F)r_i^2]}{N_{\text{obs}} - N_F}}. \quad (6)$$

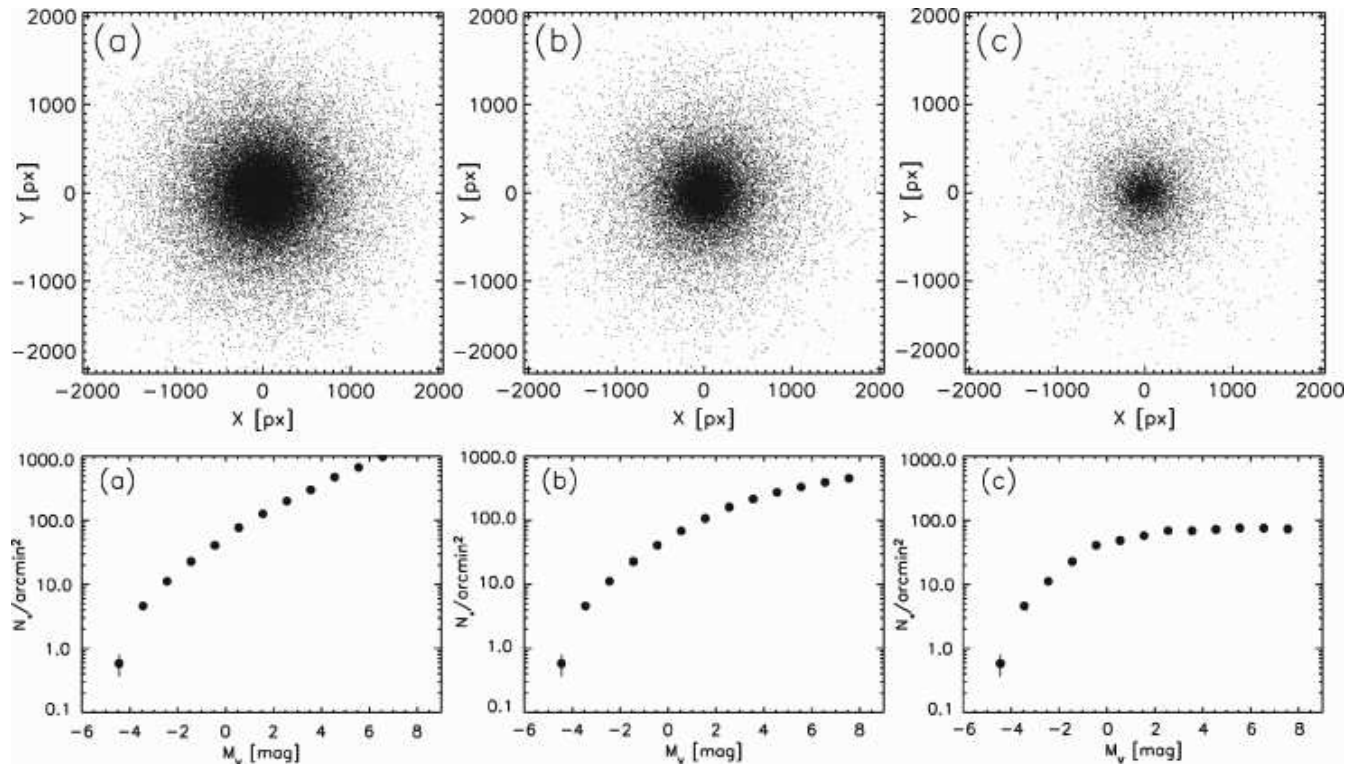


FIG. 1.— Sample of three different simulated star clusters using Monte Carlo simulations. The maps of the star clusters, which differ in their luminosity functions, are shown in the top panel. The corresponding LFs are shown in the bottom panel. All clusters were assumed to follow a King density profile and to have the same tidal radius of 0.2 . They are also similarly segregated. The LFs shown are in agreement with the results of various authors on star clusters in the MCs.

However, this simplified approach assumes that the field stars are more or less homogeneously distributed within the boundaries of the cluster, which does not correspond to reality. Specifically, Eq. (6) weighs the contribution of each star to the sum of r_i^2 by the probability, $(1 - F)$, that it is a cluster member. Still, cluster members are by their very nature more centrally concentrated, and therefore stars at smaller radii are less likely to be field stars, while those at large radii have a higher probability that they are, in fact, field stars. As a consequence, in Eq. (6) true cluster members make a smaller contribution to the Spitzer radius than they should, while the contribution of the field stars is overestimated. We verified this problem using additional Monte Carlo simulations for the construction of hypothetical background-field populations. For these simulations, the use of a specific field LF was the only constraint considered.

We constructed homogeneously distributed stellar populations with LFs typical for the background fields of both Magellanic Clouds, based on *HST* observations (e.g., Elson et al. 1997; Holtzman et al. 1999; Dolphin et al. 2001; Smecker-Hane et al. 2002). Subsequently, we inserted our artificial star clusters (§ 2.2) into the artificial background field. We constructed 32 different cases of four different clusters, each having four different degrees of stratification located in two different types of field (with different LFs). The application of our method to these artificial observations showed that *it is indeed very difficult to disentangle the contribution of the field* in the measured Spitzer radii on the basis of Eq. (6). Consequently, and since it is not possible to quantify the effect of the field contribution to observed stellar samples in clusters as a function of distance from the cluster center, a more

robust approach for the direct field decontamination of the observed stellar samples *before measuring the Spitzer radii* should be considered. Such a well-established method for the removal of any field contamination from the stellar samples of star clusters is based on the application of a Monte Carlo technique, which makes use of comprehensive observations of the local background field of the galaxy (e.g., Bonatto & Bica 2007). We apply such a sophisticated technique to actual *HST/ACS* observations of two SMC clusters, for the estimation of their Spitzer radii as a function of stellar magnitude, in § 3.

2.4. The Effective Radius

The method we propose for the diagnosis of stellar stratification in star clusters makes use of the observable counterpart of Spitzer radius, applied to the observed completeness-corrected stellar samples, and after the contamination of these samples by the field populations has been removed. This radius, which we will refer to as the *effective radius*, r_{eff} , is estimated for stars in specific narrow magnitude ranges; its dependence on magnitude is shown in the following sections. Eq. (5) can be reduced to the following expression and should, with all corrections properly applied, be equal to r_{Sp} . Thus,

$$r_{\text{eff}} = \sqrt{\frac{\sum_{i=1}^{N_{\text{obs,cc,ff}}} \frac{r_i^2}{C_i}}{N_{\text{obs,cc,ff}}}} \equiv r_{\text{Sp}}, \quad (7)$$

where r_i is the radial distance of the i^{th} stellar member of the cluster (after field subtraction), in a specific magnitude range. C_i is the corresponding completeness factor at its distance for

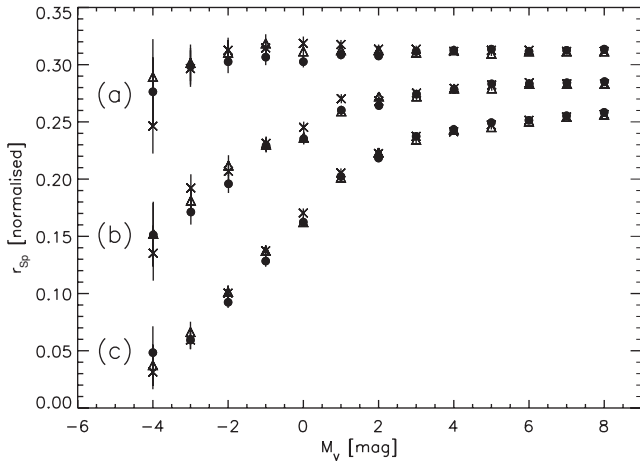


FIG. 2.— Sample of three different degrees of segregation: (a) No stellar stratification, (b) smooth stratification, and (c) for more strongly segregated bright stars. The artificial cluster shown in the middle panel of Fig. 1 is used for this demonstration. The brightest (segregated) stars appear to be confined within smaller Spitzer radii than the faint (non-segregated) stars. Different symbols for each magnitude range represent r_{SP} as it would be estimated if the cluster were observed projected onto the xy , xz , or yz plane, respectively.

the same magnitude range and $N_{\text{obs,cc,ff}}$ is the total number of observed stars corrected for incompleteness and reduced by the total number of field stars.

This radius is a statistical quantity and its estimation is rather sensitive to the number of observed stars. Therefore, the effective radius can be easily over- or underestimated if this estimation is based on few stars only, which might be the case for the brightest magnitude ranges. In order to deal with this issue, one may apply the binning in variable magnitude ranges and use wider magnitude bins toward the brighter limit, thus increasing the number of the sample stars. However, with this solution one may not be able to observe the luminosity segregation of the stars in detail. It would be more appropriate to weigh each bin by the number of sample stars as an indicator of the statistical significance of the estimation of the corresponding effective radius.

The uncertainty in the estimation of r_{eff} , as derived from Eq. (7), is mostly dependent on errors in the counting process, thus reflecting Poisson statistics. Another concern to be taken into account is the effect of projection on the estimated values for the effective radius. For non-symmetrical loose stellar systems, it is found that projection does not significantly affect the true value of the Spitzer radius (e.g., Gouliermis et al. 2000). Here, since we deal with spherically symmetric clusters, we consider the uncertainties introduced by projection for the simple case of a homogeneous density distribution.

We assume a spherical distribution of N particles ($N \gg 1$), uniformly distributed (with constant density, ρ) within a radius, R . If one observes this sphere, the distribution is not uniform anymore because of projection effects. Specifically, we investigate the size of the radius which includes half of the particles, projected along the line of sight, in relation to the radius of a sphere which – in reality – includes half of them (in 3D space). Because of symmetry we concentrate on one hemisphere, defined by the line of sight (direction of the Y axis in Fig. 3).

We define an elementary cylinder of thickness $dx = R \cos \theta d\theta$, of base radius $x = R \sin \theta$, and of height $y = R \cos \theta$ (Fig. 3). The angle θ is measured in relation

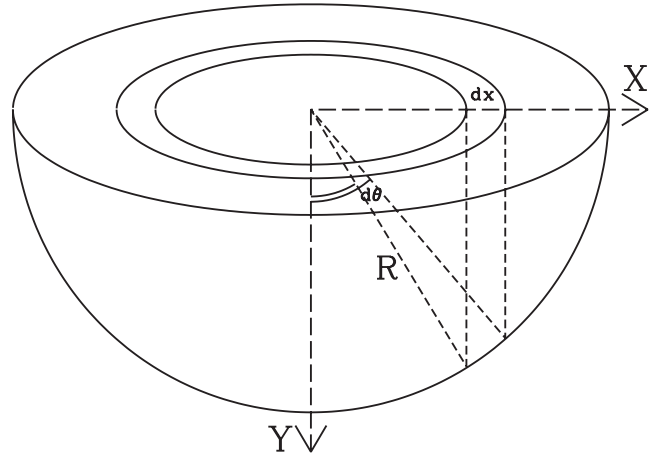


FIG. 3.— Projection of a hemispherical distribution. The Y axis coincides with the line of sight.

to the radius vertical to the surface of projection. The cylinder contains $dN = \rho dV$ particles, where V is the volume. Consequently,

$$dN(\theta) = 2\pi R^3 \rho \sin \theta \cos^2 \theta d\theta. \quad (8)$$

Integrating over $0^\circ < \theta < 90^\circ$ we expect that the number of particles included is $N = 2\pi R^3 \rho/3$. Half ($N/2$) are projected up to a limit cylinder base radius, x_h , corresponding to θ_h . This angle can be deduced from the relation

$$\begin{aligned} N/2 &= \int_0^{\theta_h} dN(\theta) = -2\pi R^3 \rho \int_0^{\theta_h} \cos^2 \theta d(\cos \theta) \Rightarrow \\ &\Rightarrow \cos^3 \theta_h = \frac{1}{2} \Rightarrow \theta_h \approx 37.467^\circ. \end{aligned} \quad (9)$$

This angle gives $x_h = R \sin \theta_h \approx 0.608R$. In reality, half of the particles are included in a volume contained within a sphere of radius $R_h = 2^{-1/3}R \simeq 0.794R$ (because of constant density). Thus, we have $R_h = 1.3x_h$. As a consequence, the proportion of the half-number radius (and consequently of the Spitzer radius, which is almost equal to the half-number radius for a relaxed stellar system) to its projected value for this distribution of particles is well-defined.

In any case, in the present study this factor is irrelevant for further analysis, since the application of a constant conversion factor to the estimated effective radii is not necessary. Moreover, this application assumes that any cluster follows a homogeneous density distribution, which is of course not always the case. Under these circumstances, we can treat the estimated effective radii used in the application of our method as the *projected* effective radii.

3. THE STAR CLUSTER SAMPLE

The proposed method for the detection of stellar stratification is designed primarily for the study of MC clusters, and therefore in the following sections we apply this method to such clusters to test its performance and to establish a consistent methodology. Moreover, in order to use the most complete available data we select clusters observed with the *HST*. The advantages *HST* introduced to crowded-field photometry in the MCs have been documented extensively by several authors since its early observations and the quality of the data obtained with both the Wide-Field Planetary Camera 2 (WFPC2) and the Advanced Camera for Surveys (ACS) has

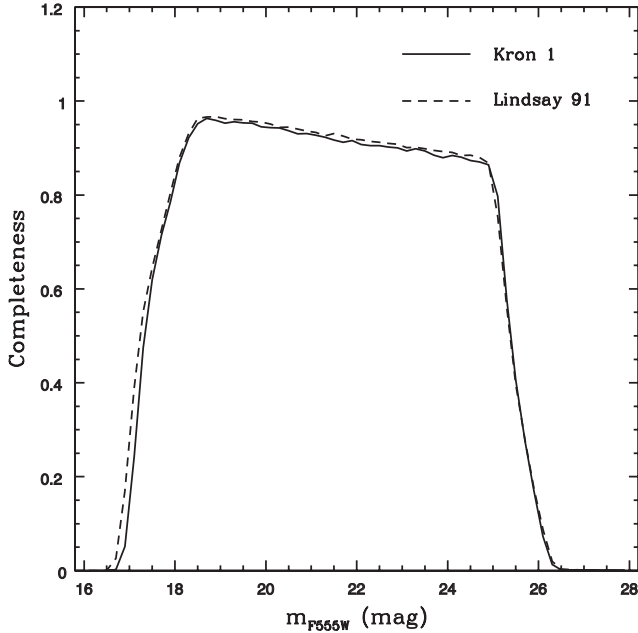


FIG. 4.— Completeness functions for Kron 1 (solid line) and Lindsay 91 (dashed line), respectively. The function has been integrated over position and color as a function of m_{F555W} .

proven to be more than adequate for detailed studies of young and old MC star clusters (e.g., Fischer et al. 1998; Johnson et al. 1999; Keller et al. 2000; Brocato et al. 2001; de Grijs et al. 2002a,b,c; Stanghellini et al. 2003; Gouliermis et al. 2004; Mackey et al. 2006; Rochau et al. 2007; Xin et al. 2008).

For the application of our new method for diagnosis of stellar stratification to real clusters we selected a set of data obtained with the ACS of the intermediate-age clusters Kron 1 (Kron 1956) and Lindsay 91 (Lindsay 1958) in the SMC. Below, we discuss the reduction of the observations of these clusters (see also Mackey & Gilmore 2004), their photometry, and the decontamination of the cluster populations from the contribution of the general background field of the galaxy using an advanced Monte Carlo technique.

3.1. Data Reduction

The SMC clusters Kron 1 and Lindsay 91 were observed with the Wide Field Channel (WFC) of ACS on-board the *HST* (program GO-9891, PI G. Gilmore). The ACS/WFC consists of two 2048×4096 -pixel CCDs, separated by a gap of ~ 50 pixels. It covers a field of view of 202×202 arcsec², with a scale of ~ 0.05 arcsec pixel⁻¹. The frames were taken in each of the F555W and F814W filters. Exposure times were 300 and 200 seconds, respectively. More details on the observations and instruments can be found in Mackey & Gilmore (2004).

The FITS files of the two clusters were retrieved from the Space Telescope Science Institute (STScI) Data Archive. The original data were reduced with the STScI pipeline, i.e., they had been bias and dark-current subtracted and divided by flat-field images. Photometry was performed with the ACS module of the package DOLPHOT¹ (Version 1.0). Photometry processes and corresponding parameters fully follow the proce-

dures and recommendation in the DOLPHOT manual. Photometric calibrations and transformations were done using the relations in Sirianni et al. (2005).

We adopted three parameters in DOLPHOT to filter the photometric results, i.e., we selected only objects with $-0.3 \leq \text{sharpness} \leq 0.3$, $\text{crowding} \leq 0.5$ mag, and $\chi^2 \leq 0.25$ in both frames. Meanwhile, we kept objects classified as good star (type 1) and star errors of types 1 to 7 by DOLPHOT, which are referred to as ‘usable’ in the DOLPHOT manual. To calculate the completeness of the photometry, DOLPHOT was run again in the artificial-star mode. For each cluster, we generated $\sim 10^6$ fake stars with limits of 16.0 - 28.0 mag in brightness and -0.50 - 2.00 mag in color. The effect of unrealistically large crowding that would lead to over-estimation of the incompleteness was taken into account by the DOLPHOT utility *acsfakelist*, which creates artificial star lists based on the original photometric catalog. The fake stars were binned in four dimensions, i.e. x and y positions, magnitude, and color. Fig. 4 presents the completeness function of Kron 1 (solid line) and Lindsay 91 (dashed line), respectively. The function is integrated over position and color and is a function of m_{F555W} . More details on the data reduction are given in Xin et al. (2008).

3.2. Field Decontamination

The observed color-magnitude diagrams (CMDs) of the ACS fields centered on Kron 1 and Lindsay 91 are shown in Fig. 5. Both fields suffer from significant contamination by field stars, as can also be seen in the corresponding maps shown in Fig. 6. Without any information about cluster-membership probabilities for the observed stars, obtained, e.g., from radial velocities and/or proper motions, the quantitative decontamination of the clusters from the field stars on a statistical basis becomes a fundamental method to obtain the CMD of the true stellar members of each cluster (see e.g. the pioneering work by Flower et al. 1980 on the LMC cluster NGC 1868).

In this work, the algorithm described in Bonatto & Bica (2007) is used for field-star decontamination of the observed CMDs of both clusters. As a first step, we use the stellar number-density profiles of the clusters to identify the radial distance from the center of each cluster, R_{lim} , where the stellar density becomes flat, indicating that the background-field density has been reached. We call this region the ‘offset region’ of the cluster. All stars in the offset regions (with $r > R_{\text{lim}}$) are treated as field stars, while the rest (with $r \leq R_{\text{lim}}$) are considered as the most probable cluster-member stars. Assuming a homogeneous field-star distribution, the number density of field stars is applied to the whole cluster region to remove the field contamination. We perform this calculation in two dimensions in the CMD, i.e., in m_{F555W} and in $(m_{F555W} - m_{F814W})$, considering also the observational uncertainties in the photometry, δ_{F555W} and δ_{F814W} .

In short, the decontamination process is done as follows: (i) we divide the CMDs of the cluster and offset-region stars, respectively, in 2D cells with the same axes along the m_{F555W} and $(m_{F555W} - m_{F814W})$ directions, (ii) we then calculate the expected number density of field stars in each cell in the CMD of the offset region, and (iii) we randomly subtract the expected number of field stars from each cell from the CMD of the cluster region. In the following description we use the symbols $\chi = m_{F555W}$ and $\xi = (m_{F555W} - m_{F814W})$ to simplify the notation. Consider a CMD cell with sides and coordinates $\chi_c \pm \Delta\chi/2$ and $\xi_c \pm \Delta\xi/2$, respectively, where (χ_c, ξ_c) are the

¹ The ACS module of DOLPHOT is an adaptation of the photometry package HSTPHOT (Dolphin 2000). It can be downloaded from <http://purcell.as.arizona.edu/dolphot/>.

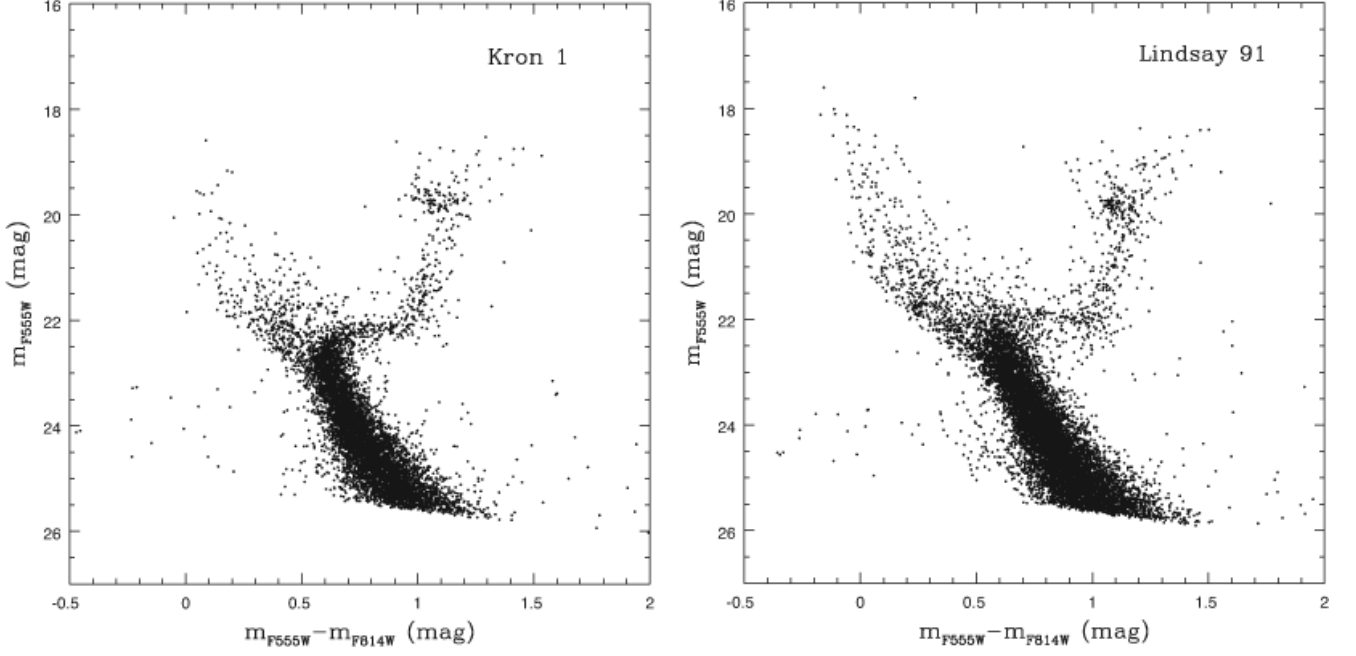


FIG. 5.— $m_{F555W} - m_{F814W}$ vs. m_{F555W} CMDs of the fields of the SMC clusters Kron 1 and Lindsay 91, observed with *HST* ACS/WFC.

cell’s central coordinates. We assume a Gaussian probability distribution to calculate the probability of a star with CMD coordinates $(\bar{\chi} \pm \delta_{\chi}, \bar{\xi} \pm \delta_{\xi})$, with $\delta_{\xi} = (\delta_{F555W}^2 + \delta_{F814W}^2)^{1/2}$, to be found in the cell, and therefore the computations take into account both magnitude and color uncertainties, for example,

$$P(\chi, \bar{\chi}) = \frac{1}{\sqrt{2\pi}\delta_{\chi}} e^{-(1/2)[(\chi - \bar{\chi})/\delta_{\chi}]^2}. \quad (10)$$

The expected field-star number density (ρ_{fs}^{cell}) in a cell is given by summing up the individual probabilities (P_{fs}^{cell}) of all offset-field stars (N_{fs}) in the cell, divided by the offset area (A_{fs}), i.e., $\rho_{fs}^{cell} = P_{fs}^{cell}/A_{fs}$, where

$$P_{fs}^{cell} = \sum_{i=1}^{N_{fs}} \int \int P_i(\chi, \chi_i; \xi, \xi_i) d\chi d\xi. \quad (11)$$

$P_i(\chi, \chi_i; \xi, \xi_i)$ is the probability of the i^{th} field star, with CMD coordinates $(\bar{\chi}, \bar{\xi})$ and uncertainties $(\delta_{\chi_i}, \delta_{\xi_i})$, to have the magnitude and color (χ, ξ) . The integral is carried out in the two dimensions, $\chi_c: \Delta\chi/2 \leq \chi \leq \chi_c + \Delta\chi/2$, and $\xi_c: \Delta\xi/2 \leq \xi \leq \xi_c + \Delta\xi/2$, respectively. In the same manner we calculate the number density of the observed stars in the cell in the cluster-region CMD, $\rho_{obs}^{cell} = P_{obs}^{cell}/A_{cl}$, where A_{cl} is the projected area of the cluster region ($r \leq R_{lim}$). Therefore, the expected number of field stars in the cell in the cluster-region CMD is $n_{fs}^{cell} = (\rho_{fs}^{cell}/\rho_{obs}^{cell}) \times n_{obs}^{cell}$, where n_{obs}^{cell} is the number of observed stars (at $r \leq R_{lim}$) located in the cell. The number of probable cluster member stars in the cell will be $n_{cl}^{cell} = n_{obs}^{cell} - n_{fs}^{cell}$, and the total number of cluster member stars is the sum of all n_{cl}^{cell} , i.e., $N_{cl} = \sum_{cell} n_{cl}^{cell}$.

To minimize any artificial effect intrinsic to the method, we apply the algorithm many times using different cell sizes ($\Delta\chi$, $\Delta\xi$) and derive different decontamination results, from which we calculate the probability of a star to be identified as a ‘true’ cluster member. Finally the field-star-decontaminated CMD

of the cluster contains the N_{cl} stars with the highest probability of being cluster members. Fig. 7 shows the corresponding CMDs of the cluster region (left panel), the offset region (central panel), and the final field-star-decontaminated CMD (right panel) for both clusters.

4. APPLICATION OF THE DIAGNOSTIC METHOD

The proposed method for the diagnosis of stellar stratification is based on the assumption that the *effective radius* of stars in a specific magnitude (or mass) range will be a unique function of this range if the system is segregated. In this section we apply our new method for the detection and quantification of stellar stratification to the intermediate-age clusters Kron 1 and Lindsay 91. Before the application of our diagnostic method and to check if the clusters are segregated, we investigate the stellar stratification using one of the most accurate ‘classical’ methods, the radial dependence of the cluster LFs and MFs.

In the previous section we showed that both clusters are evolved, by virtue of the presence of clear red-giant branches (RGBs) and red clumps in their CMDs. However, in the corresponding ‘clean’ CMDs, obtained after decontamination of the cluster stellar samples by the field populations, shown in Fig. 7 (right panels), it can be seen that there are stars at the upper main sequence (MS) and just above the MS turn-off, which are not sufficiently removed from the observed CMDs. These stars are most probably members of the younger SMC field, to which both clusters belong, and they will not be considered in the following analysis. As a consequence, in the investigation presented here, we use only the lower-MS population below the turn-off of each cluster and that of the RGB.

4.1. Stellar Stratification in the selected clusters

In this section we apply the most effective *classical* diagnostic method developed in the past for the investigation of stellar stratification to our ACS photometry of Kron 1 and Lindsay 91, to check if the clusters are indeed segregated.

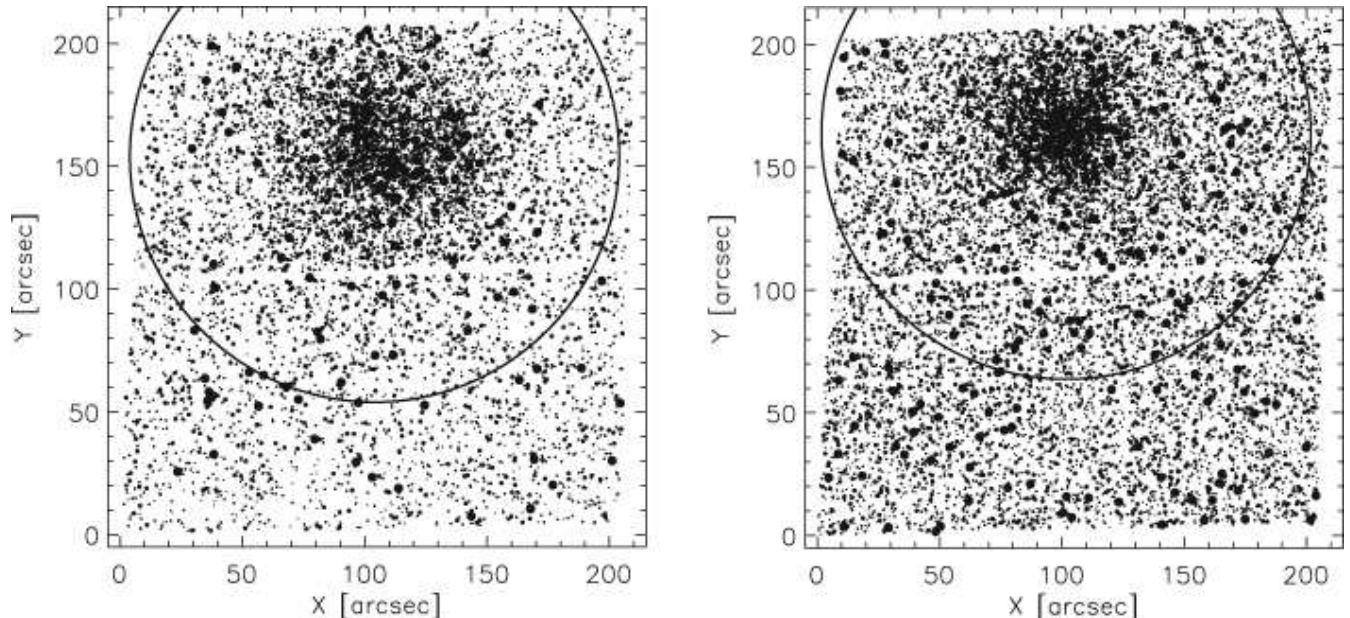


FIG. 6.— The observed ACS/WFC fields of view of Kron 1 (left) and Lindsay 91 (right). The overlaid circles have radii, R_{lim} , corresponding to the boundary between the clusters and the general field. They were defined based on the clusters' surface density profiles, as the distance from the cluster center where the density profiles become flat (see § 3.2).

This well-applied method requires the construction of the cluster LF and/or the MF and the investigation of its radial dependence. If the cluster is indeed segregated then the appearance of more massive stars toward its center will result in a shallower MF at smaller radii. De Grijs et al. (2002b) present the difficulties in the construction of an accurate MF based on the use of different ML relations and stress the differences in the MF slopes obtained. Moreover, significant numerical biases in the determination of the slope of the MF using linear regression are found if the construction of the MF was made from uniformly binned data (Maíz Apellániz & Úbeda 2005), implying the presence of systematic errors in the slopes of MFs calculated in this way.

Gouliermis et al. (2004) argue that the investigation of any radial dependence of the MF slope is not as straightforward as it seems, since any such dependence is rather sensitive to the selection of the radial distances being considered. Although stellar stratification can be identified from the cluster LF, its quantification is quite difficult because the approximation of the LF with a single power law, which is the usual approach, can only give very rough results. In any case, we apply this diagnostic to our data, in order to identify stellar stratification in our clusters and to be able to compare the results of a well-established classical method with those of our method.

4.1.1. Radial Dependence of LFs and MFs of the Clusters

In this section we examine the dependence of the shape and slope of the stellar LF on position within the clusters. We basically use the cluster LFs as smoothing functions of the full 2D (m_{F555W} , $m_{\text{F555W}} - m_{\text{F814W}}$) CMDs shown in the right-hand panels of Fig. 7. In Fig. 8 we show all annular cluster LFs out to $r = 100.0''$, corrected for the effects of incompleteness and background contamination at each respective annular radius. We carefully considered the optimal radial ranges to be used for our LF analysis, which was in essence driven by the need to have statistically significant *and* similar (cf. Maíz Apellániz & Úbeda 2005) numbers of stars in

each of the subsamples used for our comparison of the different annular LFs. For reasons of clarity, we did not normalize the LFs to the same sampling area since this would result in smaller separations among the various curves, hence hampering our assessment of any radial dependence of the LF *shape* (at this point we are not interested in the absolute numbers of stars per unit area).

We note that for a proper comparison of the annular LFs in Fig. 8 one should only consider the magnitude range in between the vertical dotted lines. For brighter stars, stochasticity in the stellar LFs starts to dominate, while the LFs are also significantly affected by the presence of red-clump stars, which are clearly visible in both CMDs. For fainter stars our subsamples are significantly statistically incomplete, at $<50\%$. On the basis of a casual comparison of the annular LFs in Fig. 8, we conclude that there is little evidence for luminosity segregation in Kron 1, although there is a hint of a flattening of the LFs towards smaller radii, particularly for $m_{\text{F555W}} \gtrsim 22.5$ mag. Lindsay 91, on the other hand, exhibits clear signs of luminosity segregation for most of the magnitude range of interest.

The conversion of an observational LF in a given passband i , $\phi(M_i)$, to its associated MF, $\xi(m)$, is not as straightforward as often assumed (see, e.g., de Grijs et al. 2002b). The differential present-day stellar LF, $dN/d\phi(M_i)$, i.e. the number of stars in the absolute-magnitude interval $[M_i, M_i + dM_i]$, and the differential present-day MF, $dN/d\xi(m)$, i.e. the mass in the corresponding mass interval $[m, m + dm]$, are related through $dN = -\phi(M_i)dM_i = \xi(m)dm$, and therefore

$$\phi(M_i) = -\xi(m) \frac{dm}{dM_i}. \quad (12)$$

Thus, to convert an observational LF into a reliable MF, one needs to have an accurate knowledge of the appropriate ML – or mass–absolute-magnitude – relation, dm/dM_i (for a detailed discussion, see de Grijs et al. 2002b). In fact, it is the *slope* of the ML relation at a given absolute magnitude that determines the corresponding mass, which is therefore quite

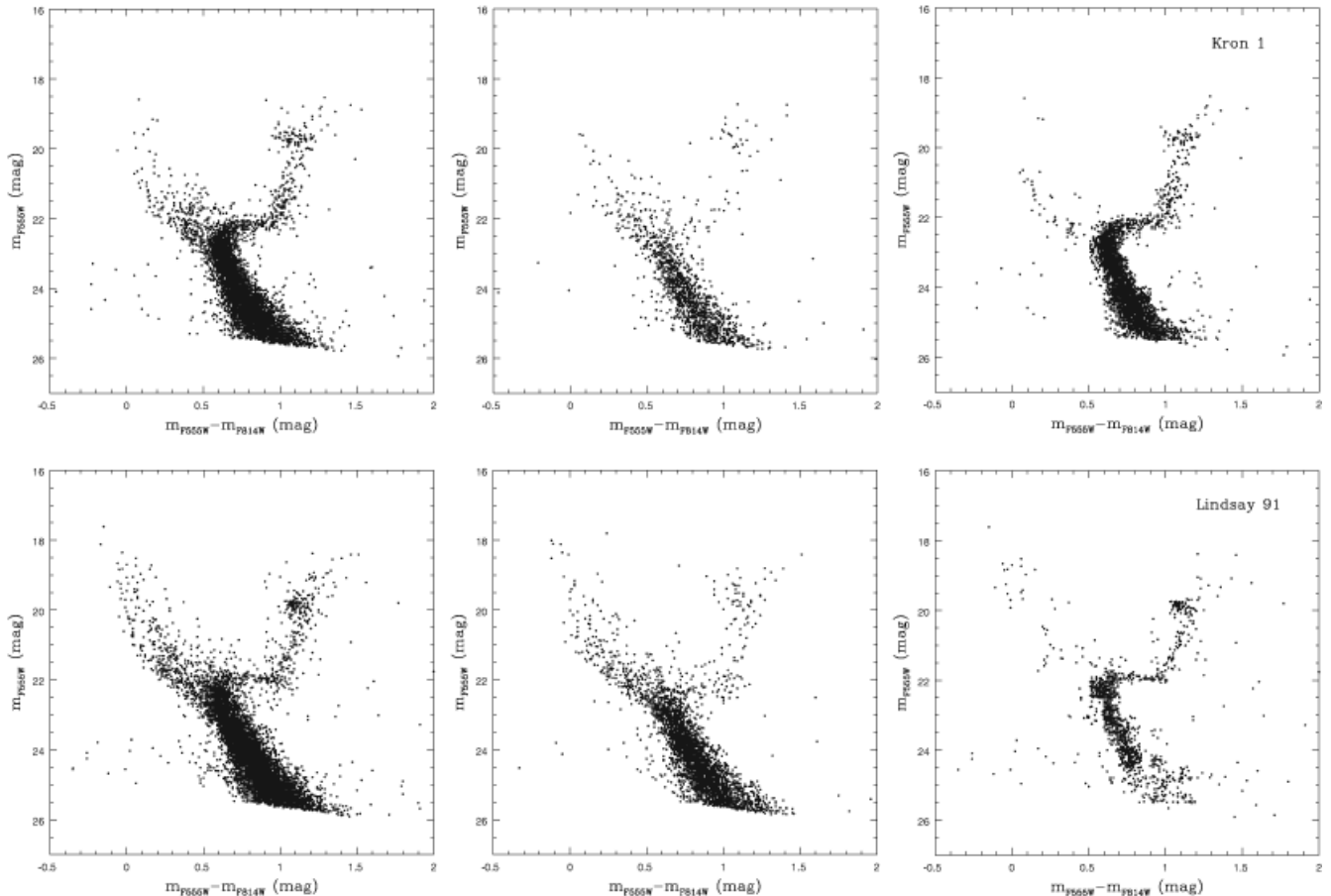


FIG. 7.— CMDs of the cluster regions ($r \leq R_{\text{lim}}$; left panel), the offset regions ($r > R_{\text{lim}}$; central panel), and the final CMDs of the clusters after field-star decontamination (right panel) for both Kron 1 (top) and Lindsay 91 (bottom).

model dependent. This has been addressed in detail by, e.g., D’Antona & Mazzitelli (1983), Kroupa et al. (1990, 1993), Elson et al. (1995) and Kroupa & Tout (1997). Given the non-linear shape of the ML relation (de Grijs et al. 2002b) and the small slope at the low-mass end, any attempt to model the ML relation by either a polynomial fit or a power-law dependence will yield intrinsically unreliable MFs (cf. Elson et al. 1995, Chabrier & Méra 1997), in particular in the low-mass regime. This model dependence is clearly illustrated by, e.g., Ferraro et al. (1997) and de Grijs et al. (2002b), who compared the MFs for their sample clusters derived from a variety of different ML relations at that time available in the literature. Nevertheless, for the sake of our discussion on mass segregation in our two sample clusters, we only need to consistently apply *the same* ML relation to the clusters’ annular LFs; any differences in the resulting MF shapes will then be due to intrinsic differences in the stellar mass distributions as a function of radius in the clusters.

In addition, the true structure of the CMD above the MS turn-off is very complex. Stellar populations of different masses overlap in color-magnitude space, so that unambiguous mass determination from isochrone fits, for the few dozen stars populating these areas in each cluster, is highly model-dependent. On the other hand, while different evolutionary models differ in terms of absolute calibration of the mass-luminosity relation, they show a quite good agreement in terms of relative mass distribution in well established evolu-

tionary phases. In any case, in a differential analysis such as presented here, the uncertainties involved in the mass determinations of the evolved stars are too large and systematic, so that we cannot include these stars in our MF analysis. Therefore, we used all stars below the MS down to the 50% completeness limit of the data. After applying the appropriate distance modulus to obtain absolute magnitudes, for our luminosity-to-mass conversions we used the updated Padova isochrones (Marigo et al. 2008; available from <http://stev.oapd.inaf.it/cmd>) for the appropriate *HST* photometric system, the metallicity and age of the cluster, and a Kroupa (1998) IMF corrected for the presence of a binary population, as suggested for use with the web interface. For the metallicity and age of both Kron 1 and Lindsay 91 we used $Z = 0.001$ (where $Z_{\odot} = 0.020$) and an age of 6.3 Gyr; their distance moduli are $m - M = 19.34$ mag and $m - M = 19.10$ mag, respectively. These physical parameters are derived from fitting the isochrone model that best matches the observed features of the CMD of each cluster.

The MS turn-off magnitude in both Kron 1 ($m_{F555W} \simeq 22.3$ mag) and Lindsay 91 ($m_{F555W} \simeq 22.1$ mag) corresponds to a mass of $\log(m_*/M_{\odot}) \simeq -0.009$, while the 50% completeness limits correspond to $\log(m_*/M_{\odot}) = -0.2$ and -0.17 for these clusters, respectively. In Fig. 9 we show the derived MF slopes as a function of cluster radius for our adopted ML conversion in the full mass range; the canonical Salpeter slope would be $\alpha = -2.35$ in this representation.

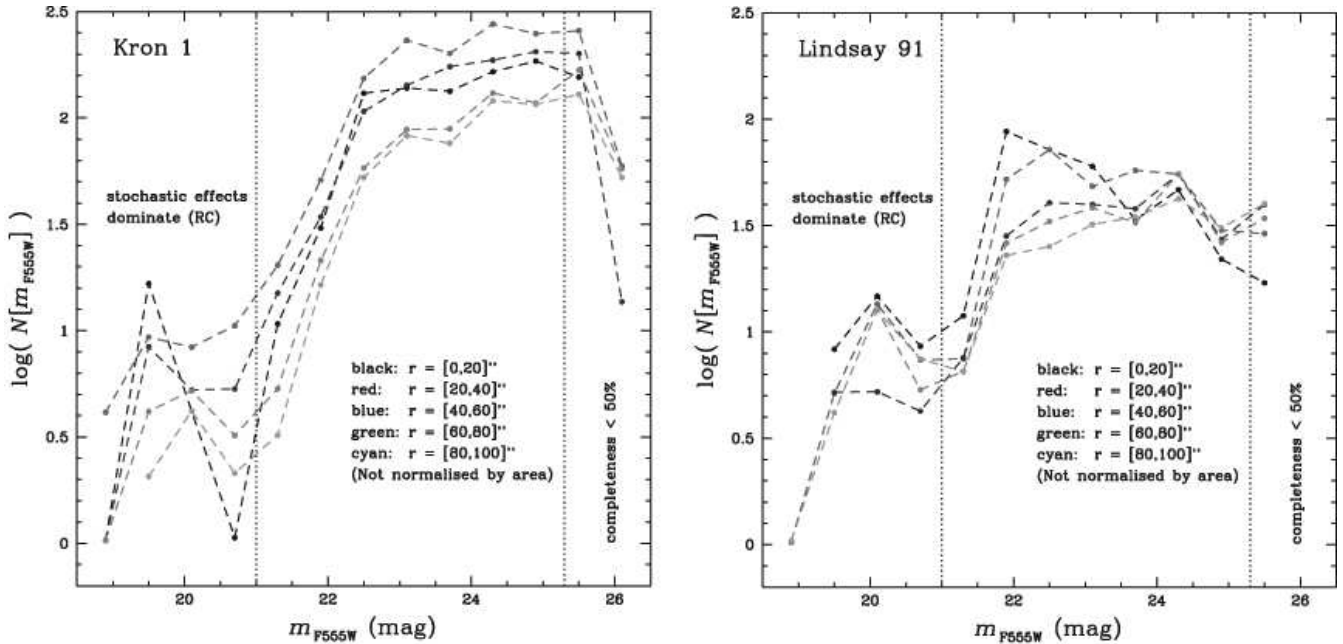


FIG. 8.— Completeness-corrected LFs of Kron 1 (left) and Lindsay 91 (right) within different annuli around the center of the clusters. These LFs clearly show how difficult it is to derive a single slope for the entire LF to compare the results for different clusters. Specific parts of the LF can, however, be approximated by a single power law. The LF of Kron 1 does not show any prominent dependence on the radial distance. Lindsay 91, however, shows a clear radial dependence of its LF in the magnitude range $22.0 \lesssim m_{F555W}/\text{mag} \lesssim 25.0$. One should only consider the LFs in the magnitude range in between the vertical dotted lines, as the brightest stars are affected by small-number statistics and the presence of a red clump (RC), while the lowest-luminosity stars suffer from significant statistical incompleteness.

The adopted radial ranges for our annular MFs are indicated by the horizontal ‘error’ bars. The vertical error bars represent the formal uncertainty in the fits. Although the uncertainties are large, both clusters seem to be affected by mass segregation, with Lindsay 91 being most obviously mass segregated, out to at least $r \sim 80''$.

4.2. Effective Radii of the Clusters

We calculated the effective radii of the stars in different magnitude ranges for both clusters. Magnitude bins of various sizes were tested and we found that a reasonable bin size, which provides good statistics and allows for the detailed observation of the dependence of r_{eff} on magnitude, is 0.5 mag. We calculated the effective radii of the stars as a function of magnitude in the F814W filter. The relations derived between the computed effective radius and the corresponding magnitude bin for both Kron 1 and Lindsay 91 are shown in Fig. 10. It is shown that, in general, the effective radius behaves as a function of magnitude for both clusters, thus providing clear indications of stellar stratification. While this behavior is more definite for the fainter stars, where it is seen that for both clusters the effective radii of these stars are larger, the uncertainties in the r_{eff} calculation for the brightest stars are rather large due to small-number statistics, and therefore no definite trend for the bright stars can be derived.

From the r_{eff} vs. magnitude plots in Fig. 10 one may conclude that the clusters exhibit stellar stratification but to a different *degree*. Moreover, from the plots in Fig. 10 one can derive the degree of stratification of the clusters in terms of the brightness range of the segregated stars, as well as the effective radius within which they are confined. Considering that a steeper slope of the relation $r_{\text{eff}}(m_{F814W})$ represents a higher degree of stratification, we conclude that Lindsay 91 is

more strongly segregated than Kron 1.

If we want to parameterize the differences between the clusters and obtain more quantitative results, we should use the two primary output parameters of our method, i.e., the *magnitude* and the *effective radius* of segregation. Both represent the limit (in magnitude range and radius, respectively) beyond which the slope of $r_{\text{eff}}(m_{F814W})$ changes significantly. However, as can be seen in Fig. 10, r_{eff} is not a monotonic function of brightness. Specifically, for Kron 1, while for stars with $m_{F814W} \lesssim 19$ mag there is a trend of r_{eff} to become larger for fainter magnitudes, this trend cannot be confirmed statistically due to large uncertainties. For fainter magnitudes, down to ~ 20.5 mag, the relation r_{eff} vs. m_{F814W} shows fluctuations and no specific trend. For even fainter stars, with $m_{F814W} \gtrsim 21$ mag, the slope of this relation shows a definite steepening as a clear indication that these stars are indeed segregated. However, this slope is still quite shallow, providing evidence of a *low degree of segregation*. A comparison between the r_{eff} vs. m_{F814W} relation of Fig. 10 for Kron 1 and the LFs of the cluster constructed for different distances from its center (Fig. 8), shows that r_{eff} seems to be a function of brightness for the entire observed magnitude range, but statistics do not allow the verification of a definite relation. Specifically, Fig. 8 shows that the LF slope seems to be distance-dependent for the full extent of the cluster and for stars within the entire observed brightness range. Indeed, a functional relation between r_{eff} and brightness seems to exist in Fig. 10 for the entire cluster, with $r_{\text{eff}} \simeq 0.7'$ for $m_{F814W} \sim 17$ mag, but this trend is not supported statistically. The small numbers of the brightest stars allow a solid statistical interpretation of this plot only for stars of $m_{F814W} \gtrsim 21$ mag. For these stars the LF slope becomes steeper outwards. The advantage of our method lies in the fact that we are able to define in a di-

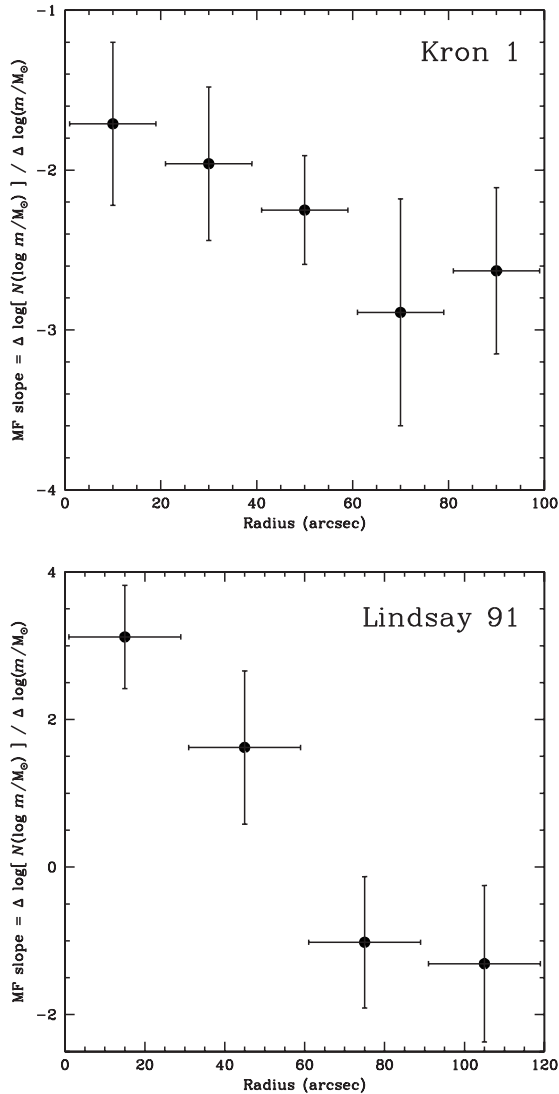


FIG. 9.— Radial dependence of the slopes of the differential MFs of Kron 1 (top) and Lindsay 91 (bottom). This dependence provides a clear indication of mass segregation of the stars on the lower MS (below the turn-off) for both clusters, and particularly for Lindsay 91. However, the uncertainties in the counting process, the model dependence for construction of the MF, and the selection of specific radial distances within which the MF is constructed for the analysis of stellar stratification introduce additional uncertainties, which work their way through to the results of this analysis.

rect manner the distance of segregation for these stars. This distance, derived from Fig. 10, is $r_{\text{eff}} \simeq 0.8'$.

For Lindsay 91 a more obvious trend of r_{eff} as a function of brightness can be seen for almost the entire observed magnitude range, $m_{\text{F814W}} \gtrsim 18.5$ mag. Also in this cluster, no clear correlation between r_{eff} and m_{F814W} is observed for the brighter stars due to their small numbers. The relation between r_{eff} and m_{F814W} can be clarified easily, however, for stars with $m_{\text{F814W}} \gtrsim 21$ mag. It is interesting to note that from the comparison of the relation of r_{eff} vs. m_{F814W} of Fig. 10 for Lindsay 91 with the corresponding LFs for different distances from the cluster center, shown in Fig. 8, we see that both plots agree that significant segregation is observed for stars with $m_{\text{F814W}} \gtrsim 21$ mag. However, specific radial distances were selected for the LFs of Fig. 8, and therefore we cannot define an accurate *distance of segregation* for these

stars, except that segregation occurs at distances $r \gtrsim 40''$. With our new method we can accurately define the distance of segregation. From Fig. 10 we derive that this distance corresponds to the effective radius of $r_{\text{eff}} \sim 0.72' \equiv 43''$, which agrees very well with the results from the LFs method, but only because of the arbitrary selection of this distance for this method.

It should be noted that the relation of r_{eff} vs. magnitude derived for the MS stars (below the turn-off) is the most reliable indicator of the degree of segregation of the studied clusters. In the case of this relation for the brighter evolved stars (above the turn-off) the situation is more complicated because the mass of these stars changes very slowly with magnitude. Specifically, according to the evolutionary models adopted here (Marigo et al. 2008) and the isochrone of 6.3 Gyr, the difference in mass of stars evolving from the base of the RGB to the AGB is much less than $0.01 M_{\odot}$, and thus the corresponding values of r_{eff} refer to extremely narrow ranges of mass per magnitude bin. As a consequence different magnitude bins correspond to roughly the same mass and the relation of r_{eff} vs. magnitude for these stars provides indications of stratification of stars of different magnitude but nearly identical mass. Naturally, this effect has consequences on the detection of *mass segregation*. In the case of the relation of r_{eff} vs. mass, the fact that the evolved stars have small mass differences can improve the number statistics, since a larger number of stars will correspond to the same mass-bins. Indeed, considering that according to the isochrone model all stars brighter than the turn-off have masses around $1 M_{\odot}$, if we group together all these stars, then we should combine the first 10 magnitude bins shown in the plots of Fig. 10 into one. The corresponding values of r_{eff} are $0.80' \pm 0.06'$ for Kron 1 and $0.88' \pm 0.07'$ for Lindsay 91; both values are quite consistent with the derived trends.

In general, based on the above, with the method for detecting and characterizing the effect of stellar stratification proposed here we can distinguish between different degrees of segregation among star clusters and compare our results from one cluster to another. The values of r_{eff} derived by using only MS stars (below the turn-off) for the studied clusters should be considered as the best tracers of mass segregation.

5. CONCLUSIONS

We present a robust new method for the diagnosis of stellar stratification in star clusters. This method uses the *effective radius*, which represents the observed Spitzer radius as estimated for various stellar groups of different magnitude (or mass) ranges in the same system. This radius is an important dynamical parameter, which approximately describes the area of gravitational influence of a given stellar group in the cluster. The proposed method detects stellar stratification in star clusters: if a cluster is segregated, then the effective radii for different stellar groups should be different from one group to another. A relation between the effective radius of every group and the corresponding selected magnitude (or mass) range can be established to consistently characterize any stratification. As a result, comparison among the results obtained for different clusters can be made.

Stellar stratification in star clusters is usually quantified based on either the surface density profiles of stars in different magnitude ranges or the cluster LF (or MF) at different radial distances from its center. Using the first method one may observe the magnitude (mass) limit for the segregated stars and using the second the radial distance where they are ob-

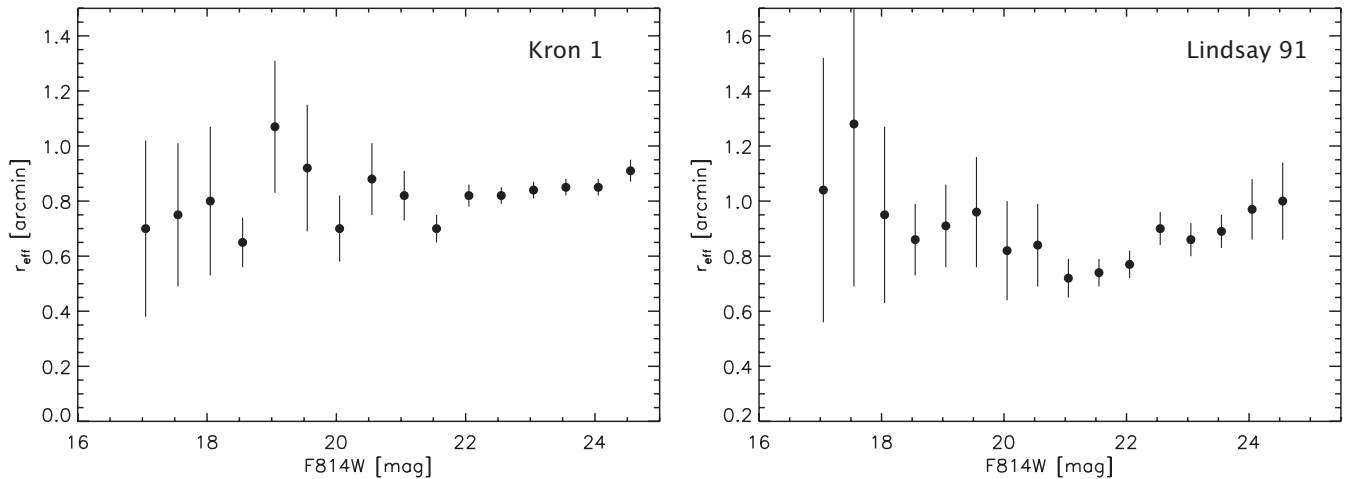


FIG. 10.— Estimated effective radii of stars within different magnitude ranges versus the corresponding mean magnitude for both clusters.

served to be segregated. Both of these results can be derived using the single application of the method proposed here. Furthermore, to apply the ‘classical’ methods for the detection of mass segregation, certain complicated fitting procedures must be applied, leading to model-dependent results. On the other hand, our method is much more straightforward in its application, and more precise in its results. This is mostly so because it is *not* necessary to (i) introduce any significant assumptions to estimate the cluster parameters, and (ii) apply any fit to parameter correlations and subsequently test the relation between the model output and the observables. Both of these steps must be applied in the classical approaches to characterize stellar stratification.

We present the application of this new diagnostic tool to two mass-segregated clusters in the SMC, observed with *HST/ACS*. The application of the new method to space-based observations helped us to establish a scheme for the comparison between the results for different clusters and to define the important parameters required to characterize stratification. These parameters are the *magnitude* and *radius of segregation*, which specify the limits beyond which segregation becomes stronger and more apparent. In addition, one may quantify the differences between clusters through the *slope of the relation between the effective radius and the corresponding magnitude range*, which can be used as an indicator of the degree of segregation of each cluster.

In each of the clusters observed with the *HST*, considered here, it was found that segregation is apparent for stars over the full observed brightness range, but small-number statistics do not allow the detection of a definite trend between r_{eff} and magnitude for several of the brightest stellar groups. A comparable *radius of segregation* is observed for stars of

$m_{\text{F814W}} \gtrsim 21$ mag in both clusters, but the *degree of segregation* seems to differ from one cluster to the other, with Lindsay 91 exhibiting a steeper function of $r_{\text{eff}}(m_{\text{F814W}})$ than Kron 1.

The continuous increase of r_{eff} as a function of brightness away from the radius of segregation up to the observed limits of the clusters shows that the fainter stars are distributed throughout a larger volume, an observation reminiscent of the ‘evaporation’ of star clusters. Still, these results are based on only two clusters and can therefore only be used rather qualitatively.

We conclude that the method we present here is simpler and more accurate than previously developed methods. This is based, first and foremost, on the more straightforward way in which the effective radius is estimated and, secondly, on avoiding any model-dependent fits. Instead, a direct correlation between the cluster’s observables is sufficient to exhibit any stellar stratification and to parameterize its significance.

D. A. Gouliermis kindly acknowledges the support of the German Research Foundation (Deutsche Forschungsgemeinschaft - DFG) through the research grant GO 1659/1-1. We thank K. S. de Boer for his contribution to an earlier version of this paper, and R. Korakitis for his comments regarding the projection of a spherical system. Based on observations made with the NASA/ESA *Hubble Space Telescope*, obtained from the data archive at the Space Telescope Science Institute. STScI is operated by the Association of Universities for Research in Astronomy, Inc. under NASA contract NAS 5-26555.

REFERENCES

- Bonnell, I. A., & Davies, M. B. 1998, *MNRAS*, 295, 691
 Bonatto, C., & Bica, E. 2007, *MNRAS*, 377, 1301
 Brandl, B., Sams, B. J., Bertoldi, F., et al. 1996, *ApJ*, 466, 254
 Brocato, E., Di Carlo, E., & Menna, G. 2001, *A&A*, 374, 523
 Brocato, E., Castellani, V., Di Carlo, E., Raimondo, G., & Walker, A. R. 2003, *AJ*, 125, 3111
 Chabrier, G., & Méra, D. 1997, *A&A*, 328, 83
 D’Antona, F., & Mazzitelli, I. 1983, *A&A*, 127, 149
 de Grijs, R., Johnson, R. A., Gilmore, G. F., & Frayn, C. M. 2002a, *MNRAS*, 331, 228
 de Grijs, R., Gilmore, G. F., Johnson, R. A., & Mackey, A. D. 2002b, *MNRAS*, 331, 245
 de Grijs, R., Gilmore, G. F., Mackey, A. D., Wilkinson, M. I., Beaulieu, S. F., Johnson, R. A., & Santiago, B. X. 2002c, *MNRAS*, 337, 597
 Elson, R. A. W., Fall, S. M., & Freeman, K. C. 1987, *ApJ*, 323, 54
 Elson, R. A. W., Gilmore, G. F., Santiago, B. X., & Casertano, S. 1995, *AJ*, 110, 682
 Fischer, P., Pryor, C., Murray, S., Mateo, M., & Richtler, T. 1998, *AJ*, 115, 592
 Flower, P. J., Geisler, D., Olszewski, E. W., & Hodge, P. 1980, *ApJ*, 235, 769
 Dolphin, A. E., et al. 2001, *ApJ*, 562, 303
 Elson, R. A. W., Gilmore, G. F., & Santiago, B. X. 1997, *MNRAS*, 289, 157
 Fischer, P., Pryor, C., Murray, S., Mateo, M., & Richtler, T. 1998, *AJ*, 115, 592

- Gouliermis, D., Kontizas, M., Korakitis, R., et al. 2000, *AJ*, 119, 1737
- Gouliermis, D., Keller, S. C., Kontizas, M., Kontizas, E., & Bellas-Velidis, I. 2004, *A&A*, 416, 137
- Hillenbrand, L. A., & Hartmann, L. W. 1998, *ApJ*, 492, 540
- Holtzman, J. A., et al. 1999, *AJ*, 118, 2262
- Johnson, J. A., Bolte, M., Stetson, P. B., Hesser, J. E., & Somerville, R. S. 1999, *ApJ*, 527, 199
- Keller, S. C., Bessell, M. S., & Da Costa, G. S. 2000, *AJ*, 119, 1748
- King, I. R. 1965, *ApJ*, 142, 387
- King, I. R. 1966, *AJ*, 71, 64
- King, I. R., Sosin, C., & Cool, A. M. 1995, *ApJL*, 452, L33
- Keller, S. C., Bessell, M. S., & Da Costa, G. S. 2000, *AJ*, 119, 1748
- Kontizas, M., Hatzidimitriou, D., Bellas-Velidis, I., Gouliermis, D., Kontizas, E., & Cannon, R. D. 1998, *A&A*, 336, 503
- Kron, G. E. 1956, *PASP*, 68, 125
- Kroupa, P. 1998, *MNRAS*, 298, 231
- Kroupa, P., & Tout, C. A. 1997, *MNRAS*, 287, 402
- Kroupa, P., Tout, C. A., & Gilmore, G. F. 1990, *MNRAS*, 244, 76
- Kroupa, P., Tout, C. A., & Gilmore, G. F. 1993, *MNRAS*, 262, 545
- Lightman, A. P. & Shapiro, S.L., 1978, *Rev. Mod. Phys.* 50, 437
- Lindsay, E. M. 1958, *MNRAS*, 118, 172
- Mackey, A. D., & Gilmore, G. F. 2003a, *MNRAS*, 338, 120
- Mackey, A. D., & Gilmore, G. F. 2003b, *MNRAS*, 340, 175
- Mackey, A. D., & Gilmore, G. F. 2004, *MNRAS*, 352, 153
- Mackey, A. D., Payne, M. J., & Gilmore, G. F. 2006, *MNRAS*, 369, 921
- Maíz Apellániz, J., & Úbeda, L. 2005, *ApJ*, 629, 873
- Marigo, P., Girardi, L., Bressan, A., Groenewegen, M. A. T., Silva, L., & Granato, G. L. 2008, *A&A*, 482, 883
- Meylan, G. & Heggge, D.C. 1997, *A&A Rev.* 8, 1
- Murray, S. D., & Lin, D. N. C. 1996, *ApJ* 467, 728
- Pandey, A. K., Mahra, H. S., & Sagar, R. 1992, *Bulletin of the Astronomical Society of India*, 20, 287
- Plummer, H. C. 1911, *MNRAS*, 71, 460
- Rochau, B., Gouliermis, D. A., Brandner, W., Dolphin, A. E., & Henning, T. 2007, *ApJ*, 664, 322
- Sagar, R., Myakutin, V. I., Piskunov, A. E., & Dluzhnevskaya, O. B. 1988, *Bulletin of the Astronomical Society of India*, 16, 87
- Scaria, K. K., & Bappu, M. K. V. 1981, *Journal of Astrophysics and Astronomy*, 2, 215 (Corrigendum: 1981, *Journal of Astrophysics and Astronomy*, 2, 439)
- Santiago, B., Beaulieu, S., Johnson, R., & Gilmore, G. F. 2001, *A&A*, 369, 74
- Sirianni, M., Nota, A., De Marchi, G., Leitherer, C., & Clampin, M. 2002, *ApJ*, 579, 275
- Smecker-Hane, T. A., Cole, A. A., Gallagher, J. S., & Stetson, P. B. 2002, *ApJ*, 566, 239
- Spitzer, L. Jr. 1958, *ApJ*, 127, 17
- Spitzer, L. Jr. 1969, *ApJ*, 158, L139
- Stanghellini, L., Villaver, E., Shaw, R. A., & Mutchler, M. 2003, *ApJ*, 598, 1000
- Subramaniam, A., Sagar, R., & Bhatt, H. C. 1993, *A&A*, 273, 100
- Testa, V., Ferraro, F. R., Chieffi, A., Straniero, O., Limongi, M., & Fusi Pecci, F. 1999, *AJ*, 118, 2839
- Xin, Y., Deng, L., de Grijs, R., Mackey, A. D., & Han Z. 2008, *MNRAS*, 384, 410